73rd International Astronautical Congress (IAC), Paris, France, 18-22 September 2022

IAC–22–C1.8.9-x74213

LEVERAGING WEAK-STABILITY BOUNDARIES FOR LIBRATION POINTS ESCAPES AND DISPOSAL

Enrico Bassissi*, Andrea Pasquale†, Michéle Lavagna‡
Dipartimento di Scienze e Tecnologie Aerospaziali (DAER), Politecnico di Milano, Italy

In the near future, the exploitation of the cislunar environment will open the frontier of space for increasingly daring and challenging explorations. Low energy transfers in this context have a fundamental role, especially when the objective is to reduce at the most the propellant use and to enable new classes of missions. In fact, leveraging the gravity of the Earth, Moon and the Sun,[16] allows to construct transfers which are particularly efficient, although with an increase in complexity and sensitivity. The objective of this work is to exploit low-energy transfers to efficiently escape the cislunar space. First, escape trajectories from the Earth-Moon Libration Point L_2 are built in the Bi-Circular Restricted Four-Body Problem (BCR4BP) framework,[18] accounting for the Sun-Earth-Moon-probe interaction, and the trajectories with the desired characteristics are saved in a database. Secondly, a clustering step is performed, employing dynamical systems theory to gain insights embedded in the BCR4BP dynamical flow, to reduce the dimension of the database and extract the different escape trajectories families as a function of the design variables used. Then, an initial condition generator based on the database and on numerical patching technique is implemented, giving the possibility to construct initial guesses once the desired heliocentric transfer toward Near Earth Asteroids is assigned. The methodology is deeply tested and its strengths and weaknesses are highlighted and discussed.
keywords: Weak-Stability Boundaries, Multi-Body Dynamics, Machine Learning, Clustering, Escape Trajectories

1. INTRODUCTION

The scientific and commercial exploitation of the cislunar environment for both manned and unmanned missions will increase in the next few decades, opening the frontier of space for increasingly daring and challenging explorations. Those ambitious missions face complex dynamics that cannot be adequately addressed with classical trajectory design techniques,[15] motivating instead the consideration of automated algorithmic approaches more traditionally associated with the fields of multi-body dynamics. In this context the Earth-Moon Lagrangian Point L_2 is gaining the attention, since it will be a new base for long-duration habitation: it is where the future Lunar Orbital Platform-Gateway (LOP-G) will be placed and it will become a possible departing outpost for different types of exploration missions, including Near-Earth Asteroids, missions to Mars or other objects in the Solar System. New methodologies for trajectory design in multi-body environment have to be leveraged, pushing the boundaries toward new processes and techniques. For example, the low-energy trajectory design represents one of the promising directions of future developments. Weak Stability Boundaries (WSB) theory[1,2,4] takes full advantage of the dynamic effects of two or more gravitating bodies, and it has been already employed in some missions during the last few decades, such as HITEN,[22] SMART-1,[6] ARTEMIS,[3] GRAIL[17] and others.

The paper will focus on escape trajectories from the Cislunar space, which has already being studied by different authors[5,13],[20] characterising their dynamical behaviour in two/three and four-body problem and addressing the problem to design a transfer from the Earth-Moon Libration Points to a destination object outside the cislunar environment.

Techniques from unsupervised machine learning may aid in summarising and understanding the solution space inferring undetected patterns, and improve the visualisation of higher-dimensional data, as done by Smith and Bosanac[19] with the specific application of identifying a set of motion primitives that represents a family of orbits.

This paper work will expand on these trajectory design research topics, trying to leverage and exploit weak stability boundaries in the Sun-Earth-Moon BCR4BP framework in order to obtain initial guess low energy escape trajectories from the cislunar space, in a reversed WSB approach. It will

*enrico.bassissi@mail.polimi.it
†andrea.pasquale@polimi.it
‡michelle.lavagna@polimi.it

build upon the structure already defined in literature, trying to expand the application of Machine Learning topics to astrodynamics purposes. In particular the knowledge about unsupervised clustering of open (escape) trajectories by exploiting geometrical and parametric features, in a complex and sensitive environment such as BCR4BP, applying the weak stability boundaries theory to a case study scenario related to escape the cislunar environment to reach Near Earth Asteroid.[9]

The details of the modelling instruments, processes or numerical methods used will be described within the sections. The considerations and results are disseminated incrementally in the sections and grow from the previous block knowledge and reviews. The paper is organised as follows:

- In **section 2**, the BCR4BP dynamical model and the reference frames used in the study are presented.
- In **section 3**, the procedure for dividing Inner and Outer trajectory sets generation is also presented. The first analysis related to the generation of the WSB trajectory is described and performed, with an initial pre-process filtering of the large amount of data produced.
- In **section 4**, the Machine Learning Clustering is applied to the dataset, presenting the division in Families resulting from the process.
- In **section 5**, the Initial Guess Generator pipeline is presented, a NEA case study is devised, and the most relevant results are shown.
- In **section 6**, the conclusions are presented.

2. Models and Methods

2.1 *Bi-Circular Restricted Four-Body Problem*

In this paper, the design of trajectories in the cislunar space is performed leveraging to the Bi-Circular Restricted Four-Body Problem, or BCR4BP.

When the motion of the massless particle is assumed to be influenced by the gravitational pull of three bodies instead of two, such as in the context of the trajectory design in the Sun-Earth-Moon system, the Four-Body problem is exploited. This model assumes that the two primaries P_1 and P_2 revolve in circular orbits about their barycentre (B_1) and B_1 moves in circular orbits around the centre of mass of the whole system, B_0.

The BCR4BP can be seen from two different but identical frame: one taking as reference the Sun-Earth system and the other synodic with Earth-Moon system. Consequently, the equations of motion can be written in the Sun-Earth synodic frame or in the Earth-Moon one.[18]

In the first case, the equations of motion considers the the Moon as a perturbation of the Sun-Earth CR3BP as in fig. 1, and can be derived from a pseudo-potential function ($\underline{\Upsilon}$), reported in eq. (1) and continuing in eq. (2). Here, and in the following equations, $\dot{(\cdot)}$ and $\ddot{(\cdot)}$ denotes the first and the second derivatives with respect to the non-dimensional time and $\partial(\times)/\partial(\cdot)$ indicates the partial derivative of a function $(\times)$ with respect to a variable $(\cdot)$. The terms in the equations are: θ_{EM} is the Moon angular position which respect to the Sun-B_1 $\underline{x}$ synodic axis; $\underline{\mu}$ denotes the mass ratio of the Sun-(Earth+Moon) CR3BP and with $\tilde{\mu}$ the one of the Earth-Moon CR3BP; and r_{43}, r_{13}, and r_{23} represents this time respectively the distance of the particle from the Sun, the Earth and the Moon.

$$\underline{\Upsilon} = \frac{1}{2}(\underline{x}^2 + \underline{y}^2) + \frac{1-\underline{\mu}}{r_{43}} + \frac{\underline{\mu}(1-\tilde{\mu})}{r_{13}} + \frac{\underline{\mu}\tilde{\mu}}{r_{23}} \quad [1]$$

$$\begin{cases} \ddot{\underline{x}} = 2\dot{\underline{y}} + \dfrac{\partial \underline{\Upsilon}}{\partial \underline{x}} \\ \ddot{\underline{y}} = -2\dot{\underline{x}} + \dfrac{\partial \underline{\Upsilon}}{\partial \underline{y}} \\ \ddot{\underline{z}} = \dfrac{\partial \underline{\Upsilon}}{\partial \underline{z}} \end{cases} \quad [2]$$

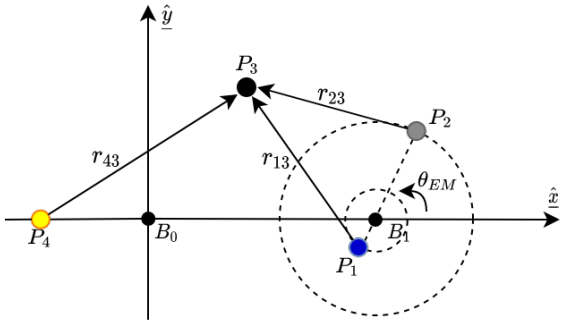

Fig. 1: BCR4BP SB1 Frame Depiction.

The other formulation of the BCR4BP, instead, considers the Sun as a perturbation of the Earth-Moon CR3BP. In this case, the equations of motion can be written in the Earth-Moon synodic frame, reported in eq. (4), which can be derived from the pseudo-potential function ($\tilde{\Upsilon}$) in eq. (3). The terms shown in the equations are: $\tilde{r}_{13}$, $\tilde{r}_{23}$ and $\tilde{r}_{43}$ representing respectively the distance of the particle from the Earth, Moon and Sun; θ_S is the Sun angle measured counterclockwise from the Earth-Moon x synodic axis and a_S the scaled Sun distance; $\tilde{\mu}$ is the Earth-Moon mass ratio and $\tilde{m}_S$

the non-dimensional mass of the Sun.

$$\tilde{\Upsilon} = \frac{1}{2}(\tilde{x}^2+\tilde{y}^2) + \frac{1-\tilde{\mu}}{\tilde{r}_{13}} + \frac{\tilde{\mu}}{\tilde{r}_{23}} + \frac{\tilde{m}_S}{\tilde{r}_{43}} - \frac{\tilde{m}_S}{a_S^2}(\tilde{x}\cos(\theta_S)+\tilde{y}\sin(\theta_S)) \quad [3]$$

$$\begin{cases} \ddot{x} = 2\dot{\tilde{y}} + \dfrac{\partial\tilde{\Upsilon}}{\partial\tilde{x}} \\ \ddot{y} = -2\dot{\tilde{x}} + \dfrac{\partial\tilde{\Upsilon}}{\partial\tilde{y}} \\ \ddot{z} = \dfrac{\partial\tilde{\Upsilon}}{\partial\tilde{z}} \end{cases} \quad [4]$$

2.2 *Frames*

- **ECLIPJ2000**: it's the realisation of the Mean ecliptic and equinox of J2000 and it is the inertial reference frame used in this work, that can be centred at any point of interest, such as the Earth, the Sun, the Moon, etc...
- **EM-SYN**: it's, as its name indicates, a rotating frame with origin at the barycentre of the Earth-Moon system. The x axis is always directed from the Earth to the Moon as the primaries orbit their barycentre, the z axis is normal to the plane of motion of the primaries and the y axis completes the orthonormal triad. It is an instantaneous synodic frame associated to the Earth-Moon CR3BP. It is a two-vectors frame built up with the instantaneous Moon position and velocity about the Earth as taken from *SPICE de440* ephemerides.
- **SE-SYN**: the x axis is now directed from the Sun to the Earth, and the origin is the barycenter of the Sun-Earth system. It is the instantaneous synodic frame associated to the Sun-(Earth+Moon) CR3BP. In analogy with the EM-SYN frame, it is a two-vectors frame built up with the instantaneous Earth-Moon Barycenter position and velocity about the Sun as taken from *SPICE de440* ephemerides.

3. Initial Conditions Generator

3.1 *Control Surface*

To design the trajectories under discussion, the problem has been splitted into two separated regions, decoupling the design of the escape between the Earth-Moon region and the interplanetary trajectory leg toward the target. Therefore those two regions can be defined as follows.

- **Inner Problem**: starting from the departure point up to a given Control Surface radius (R_c), is the cislunar leg of the trajectory. In the case under discussion, from L_2 Libration Point, or from orbits around it, and include one or multiple flybys of the Earth or the Moon.
- **Outer Problem**: is associated to the heliocentric leg of the trajectory, from the selected Control Surface radius up to the target interception.

This idea is built upon the similar concept developed in literature of the Sphere of Equivalence (SOE) by other authors,[7] that represents a mathematical surface where the Inner Problem-model gravity vector field is equivalent to a two-body vector field. However, the switching surface exploited in this work is an abstract concept, not a physical one: to guarantee a symmetric patching, a spherical surface is considered as switching surface. Introducing this simplification allows to remove the direct dependency on θ_{EM}, enabling the possibility to generate Outer Problem and Inner Problem arcs independently. A switching surface, centred in the Earth-Moon Barycenter B1 with radius approximately $2 \cdot SOI_{Earth-Moon} = 2 \cdot 145 \cdot R_{Earth\ Equator} \cong 2 \cdot 10^6$ km is then considered. With this distance, also the spacecraft dynamic around the Sun-Earth Lagrangian Points L_1 and L_2 has been considered in the effective regions.

On the switching surface, vector quantities that has to be matched can be generally denoted with q^+ if belonging to the Outer Problem, and q^- if associated to the Inner Problem, as in fig. 2. From this, the η angle, between the Inner and the Outer Problem vectors can be defined as in and eq. (5) the vector difference as in eq. (6).

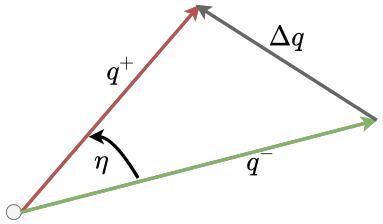

Fig. 2: General Inner-Outer Problem Vectors Patching.

$$\eta = \arccos\left(\frac{q^+ \cdot q^-}{||q^+||\,||q^-||}\right) \quad [5]$$

$$\Delta\underline{q} = \underline{q}^+ - \underline{q}^- \quad [6]$$

3.2 *Starting Point and Free Variables*

In the BCR4BP SB1 framework, L_2 is derived from the rotation of the state generated in CR3BP. In this way, L_2 moves rigidly with the Earth-Moon conjunction axis, on the other side of the Moon, so that it can be identified uniquely through the same degree of freedom of the Earth and Moon themselves, the moon angle θ_{EM}.

Analysis performed through the use of the dynamical substitute of L_2 in BCR4BP instead of the CR3BP derived L_2 led to similar results as the one presented here. Therefore

the decision to simplify the work and alleviate one more degrees of freedom at the beginning of the dynamical exploration.

The other degrees of freedom acting on the system are the impulse ΔV applied at L_2 to exit from its "equilibrium" position and α the angle at which this perturbation is applied with respect to the radial direction θ_{EM} .

The free variables are depicted in fig. 3

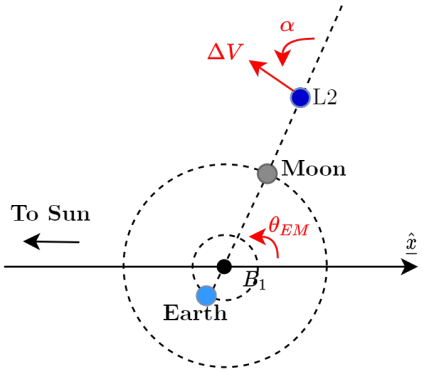

Fig. 3: In red are shown the DOFs of the problem: θ_{EM}, ΔV, α.

The ranges of evaluation in this step of the analysis are reported in table 1:

Table 1: Initial DOFs Ranges of Evaluation

θ_{EM} [rad]	Δ V [m/s]	α [rad]
$[0, 2\pi)$	$[1, 200]$	$[0, \pi/2]$

3.3 *Inner Condition Set*

These free variables permutations applied to the dynamical system at hand, have been propagated for a time span of 1 year. During the propagation, many aspects have been tracked in order to proceed with a post-processing step to prune the large amount of data and make the following steps more efficient and directed to trajectories that are already known to satisfy the constraints of the analysis to be done. The main event functions written for this work are used to find:

- **Escape**: the relevant trajectories for this analysis must lead to an escape from the Earth-Moon system. To determine which trajectories actually leave, it has been decided that the spacecraft should cross the Control Sphere distance R_c without returning in the considered time, where the spacecraft can be considered in a purely heliocentric trajectory.
- **EMB Apoapsis**: this is the method with which the WSB were detected. If the trajectory has an apoapsis in the SB1 frame of reference with respect to the Earth-Moon Barycentre B_1 in the region near the Control Sphere at 1.5/2 million km, then it's considered a valid WSB.
- **Earth/Moon Periapsis**: those encounters were considered relevant in perspective of a later analysis on manoeuvres applied along the trajectory, where a control applied at significant points, such as pericentres or apocenters, are in general more efficient than other points.
- **Crash Conditions**: only safe solutions that do not crash into the Earth or the Moon are considered, because they lead to errors in the other propagations, erratic behaviour of the dynamic and ultimately brought to non-uniform analysis in the following steps of the pipeline.

3.4 *Considerations*

The results of this initial condition pre-processing are intended to serve as filter to prune the vast number of trajectories that have been produced during the propagation step. In this way the following steps of the analysis pipeline will focus on trajectories that already satisfies the criteria needed by the objective of the work and not to the whole number of possible trajectories ever. Another objective of this phase was also to gain insights from the dynamical behaviour of the environment and understand which parameters had more or less effect on the overall analysis and focus the effort on the more relevant ones. These scopes were fulfilled: from initial results was clear that the WSB Escape trajectories were mainly reliant on θ_{EM} and ΔV degrees of freedom and α was less effective, especially at low $\Delta V < 50$ m/s, as it's possible to see in fig. 4. The meaning of this behaviour has been addressed to the fact that for lower ΔV, the impulse performs more as a perturbation and it was solely dedicated to getting out of the nominal L_2 trajectory in an almost natural evolution. For this reason the direction of application of the ΔV become less relevant, still being always positive according to the direction of motion.

Another result on the free variables analysis is that the valid WSB Escape trajectory generates only in the II and IV quadrants of the xy plane with B_1 as origin. This effect was correlated to the fact that trajectories starting in other quadrants were rapidly evolving toward direct escape and not through a WSB. This effect was also more defined and confined for the low ΔV ranges selected, whilst there

were some minor spill-off into the I and III quadrant for ΔV greater than ~ 200 m/s, as visible in fig. 4. For this reason, the θ_{EM} free variable was reduced in range span to the angular sectors of solutions existence opening the possibility of performing two different parallel analysis for the II quadrant and IV quadrant generated trajectories, that are almost symmetrical but still potentially different.

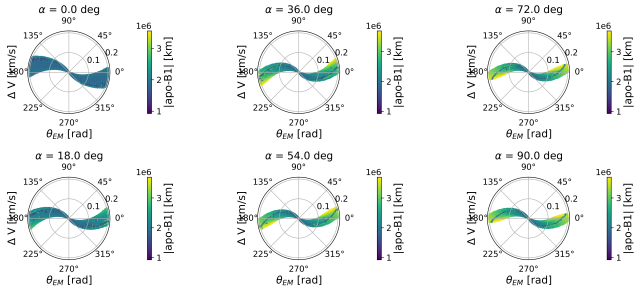

Fig. 4: WSB Escape Trajectory Existence at Varying α, Polar Plot

To summarise, the final set of free variables is given in table 2.

Table 2: DOFs Ranges of Evaluation After First Post-Processing

θ_{EM} [Quadr.]	Δ V [m/s]	α [-]
II-IV	[1, 50]	Removed

4. Machine Learning Clustering

The need of the analysis elaborated in this section of the paper comes from the fact that processing all the trajectories together can be chaotic, too much related to brute force approach, leading ultimately to inconclusive and/or unrepeatable results. The trajectories are too many to be detected and analysed as unique bunch of elements or to be separated by hands from a researcher, also in perspective of increasing number of propagations through the use of GPGPU programming applied to astrodynamics problems.[8] The best tool to approach this sort of problems is indeed Machine Learning: it enables the analysis of a large amount of data using innovative and well-studied techniques, that will be impossible to reproduce with traditional computational tools.

4.1 *DBSCAN*

In particular, in this case study machine learning is used to perform the automatic clustering of the trajectories, using a clustering algorithm, namely *DBSCAN* (Density-Based Spatial Clustering of Applications with Noise). *DBSCAN* views clusters as dense area of the vector space separated by areas of low density. As described by Scikit-Learn developers,[14] the central component to the *DBSCAN* is the concept of core samples, which are samples that are in areas of high density. A cluster is therefore a set of core samples, each close to each other (measured by some distance metric) and a set of non-core samples that are close to a core sample (but are not themselves core samples). There are two parameters to the algorithm, *min_samples* and *eps*, which define formally the concept of dense, controlling respectively the local neighbourhood of the points and how tolerant the algorithm is towards noise.

4.2 *Features Space*

A finite dataset contains n objects where each object is defined by a m-dimensional feature vector. Many parameters can be used as features for a Machine Learning algorithm training, as described in,[19] inspiration for this aspect of the research. For what concerns astrodynamical purposes and orbits clustering they can be found in the geometric realisation of the orbit, directly through the state in cartesian or spherical coordinates; the parametric structure of the orbits such as the periapsis number, position and velocity relative to both the Earth and the Moon; the time for the trajectory to reach the escape control sphere T_{R_c}; the energy related, such as the value of the Hamiltonian along the trajectory; the indices FTLE and stretching index; the sensitivities of the trajectory with respect to the free variables $\frac{\partial x^t}{\partial(\Delta V,\theta_M)}$, $\frac{\partial(r^t,\theta^t,\psi^t)}{\partial(\Delta V,\theta_M)}$.

In this work, all of the above features were tested, but in the end the geometrical ones have led to the best performances. The geometry of an orbit in BCR4BP can be represented by a variety of different feature vectors. One representation of the geometry of a planar orbit involves the normalised in-plane position with respect to B_1 and velocity components of states that are equally spaced in time along the trajectory and can be defined as in eq. (7).

$$\underline{f} = \left[\frac{(x_m - x_{B1}) - x_{min}}{x_{max} - x_{min}}, \frac{y_m - y_{min}}{y_{max} - y_{min}}, \cdots \right. \\ \left. \frac{v_{x,m} - v_{x,min}}{v_{x,max} - v_{x,min}}, \frac{v_{y,m} - v_{y,min}}{v_{y,max} - v_{y,min}} \right] \quad [7]$$

where m goes from 0 to the number of discrete positions sampled along the orbit. All the components have been normalised between the maximum and the minimum value to remain in the range [0,1]. The velocities have been considered in addition to the mere positions since after heavy testing it was cleat to be beneficial for the clustering algorithm effectiveness. Having also extra information about the velocity of the spacecraft at the evaluation points helped discriminating two similar trajectories with close positions in

space, especially while still near the Earth-Moon system, but with different velocity hence getting a glimpse of the future behaviour from early points.

4.3 *Hyper-parameters Tuning*

DBSCAN is very sensitive to the values of *eps* and *min_samples*. Therefore, it is very important to understand how to select those values. For this reason, an optimisation process has been devised in order to avoid the difficult and repetitive manual tuning of the parameters. Particle Sworm Optimization (*PSO*) algorithm was considered because it was the best performant of all the possible heuristic algorithm tested (*GA*, *DE*, *PS*), reaching convergence faster and with a better cost function result. As per the *PSO* algorithm hyper-parameters themselves, they were used some values around the default values: population size of 50 (*pop_size=50*) and maximum generation number has been set to 10 (*n_gen=10*), trade-off between getting better results and increasing the computational time required, while reaching valid results. The time required averagely on the CPU used (Intel Core i7-7500U @ 2.70GHz, 2 Core) was 17.33 minutes.

An important aspect of using Machine Learning algorithms is to not take the computer's result as given, but critically understand what the result is and how much does it make sense with respect to what is the understanding of the domain and the knowledge of the environment. A common approach is to evaluate the quality of clustering solutions. Apart from the visual inspection of the clustered result from the human researcher, a more programmatic approach involves the use of internal validity criteria, which is a technique of validation of the results using only the information intrinsic to the data. Applying this concept to density-based clustering, Moulavi, Jaskowiak and Campello in *HDBSCAN* introduced the density-based clustering validation (DBCV) index.[23] The DBCV is governed by the maximum internal sparseness of each cluster and the highest density regions between pairs of clusters. From this, the validity index can be computed and its value varies in ranges [-1, 1], with -1 being completely not valid and 1 cluster that is coherent within itself and with the other clusters. This was then selected as the performance metric to use in the optimisation process.

4.4 *Clustering Results*

A final set optimal choice of parameters is assumed to generate a clustering result with: large validity index; a low percentage of trajectories identified as noise; a moderate amount of clusters, avoiding either an excessively large or small amount of groups. The families are presented here below, divided by the quadrant of starting θ_{EM} (II or IV) to ease the readability of the results, the comprehension of the phenomena under study, and because this subdivision was the natural process of the clustering starting from the Initial Condition Generation results section 3.4.

The optimisation resulted in the best hyper-parameters *eps* and *min_samples* for *DBSCAN* to cluster the different Families departing with θ_{EM} in the II Quadrant, reported in table 3, along with the average Validity Index value obtained for the final cluster distribution (*Mean VI*) and the percentage of coverage of the datapoints clustered with respect to the totality of datapoints (*Coverage*).

Table 3: DBSCAN Hyper-parameters for F II Q

eps	***min_samples***	**Mean VI [-]**	**Coverage [%]**
0.0574	106	0.779	81.24

Following it will be shown the features space as seen by the algorithm itself, first for the positions in fig. 5 and then for the velocities fig. 6, "connecting the dots" of the progressively increasing features, where the features of each orbit are coloured based on their assigned cluster.

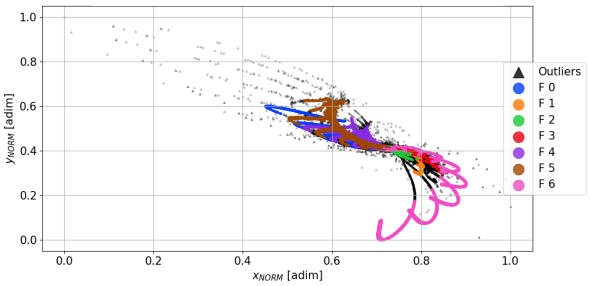

Fig. 5: Features Space in Positions for F II Q

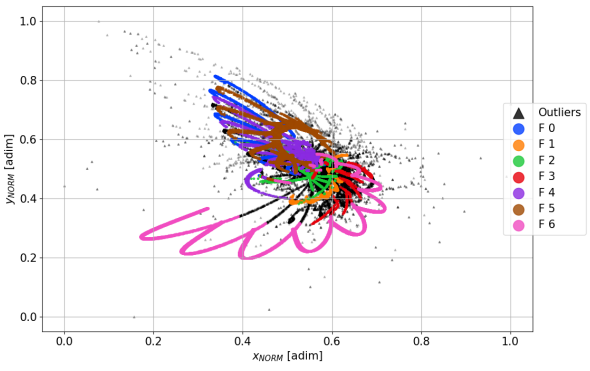

Fig. 6: Features Space in Velocities for F II Q

The final families' plot in *xy* plane are here shown in

fig. 7 as detected by the *DBSCAN* optimised algorithm. For each cluster, some thirty random trajectories taken as representatives are plotted to show the general behaviour and evolution within the family.

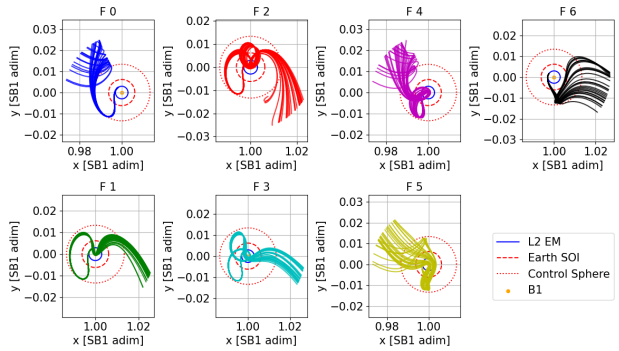

Fig. 7: *xy* plot of Families Trajectories Detected through Clustering for F II Q

Also for the Families departing with θ_{EM} in the IV Quadrant, similar features space clustering results are found with the parameters reported in table 4, and the families as detected by the *DBSCAN* algorithm are depicted through their *xy* plot in fig. 8.

Table 4: DBSCAN Hyper-parameters for F IV Q

eps	***min_samples***	**Mean VI [-]**	**Coverage [%]**
0.0437	118	0.850	80.08

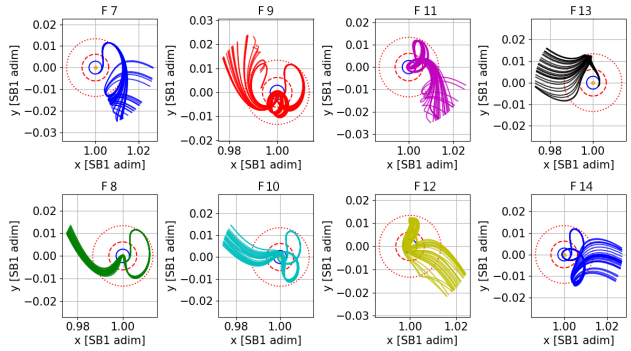

Fig. 8: *xy* plot of Families Trajectories Detected through Clustering for F IV Q

As can be seen from the plots, the variety of trajectories is high, with different geometrical and dynamical behaviours, manifestation of the complex and sensitive environment under study. These different families will be used by the Initial Guess Generator (IGG) data scan procedure to find the best match for a specific outer problem target.

It's interesting to notice that even considering only the families of the II Quadrant it's possible to reach targets of the inner and outer heliocentric space (with respect to the Earth), meaning objects that have smaller and bigger orbital semimajor axis than the Earth respectively. Obviously this span increase with the usage of the second block of trajectories.

The same geometrical and dynamical considerations can be done for both the groups, noticing that the trajectories reflect the quasi-symmetric behaviour of the BCR4BP framework.

Both the Quadrants Trajectories Sets have performed well for what concern the Validity Index metric, scoring positive and toward 1 for all the clusters. Also the noise has been successfully kept below the 20% threshold considered as maximum residual noise for a balanced optimisation.

Among the dynamical characteristics of the trajectories, the most relevant for practical purposes can be the V_∞, or hyperbolic excess velocity, the inertial velocity at infinite distance from the Earth, meaning the extra velocity on the hyperbolic escape trajectory into heliocentric space from cislunar environment. Of course it's impossible to evaluate the velocity at true infinite, but a few million km away, exactly the R_c used in this thesis work as control sphere, the actual speed is so close to V_∞, completely in radial direction, that can be considered to be equal to V_∞.

This parameter is important in this work because, among the requests made by an Outer Problem transfer trajectory, there will be for sure a demanding speed to reach some of the target objects, and the higher the natural V_∞, the more possibilities there are that with a small control manoeuvre this request will be satisfied.

All these trajectories are currently departing from L_2 Lagrangian Point, that is modelled as stationary rigid point in the Earth-Moon axis, so in a closed orbit itself, with its own $V_{\infty_{L_2}} \sim 0$, it's inertially still with respect to the Earth. Downstream the analysis, an important aspect that can be observed is that the trajectories reach on average the 1 km/s order of magnitude by only applying a small impulse perturbation at departure of the order of tens of m/s.

5. Initial Guess Generator

The final objective of this analysis is to produce an end-to-end technique to generate initial guesses for escape trajectories from cislunar environment, with embedded weak-stability boundaries features, matching an external requested condition towards NEA objects, to be later assigned

to a full multiple-shooting optimisation algorithm for final tuning.

5.1 *Targets and Case Study*

To start, a brief analysis of the NEA objects under discussion is required. To do this, a program to use NASA's Small Body DataBase (SBDB[12]) was written, getting all the characteristic parameters of this subset of objects, keeping them divided into the four main groups identified in literature:

- **Amors**: Earth-approaching NEAs with orbits exterior to Earth's but interior to Mars'.
- **Apollos**: Earth-crossing NEAs with semi-major axes larger than Earth's.
- **Atens**: Earth-crossing NEAs with semi-major axes smaller than Earth's.
- **Atiras**: NEAs whose orbits are contained entirely with the orbit of the Earth.

Since the possible targets are many and a specific asteroid is not the main objective of this thesis work, the decision made was to not choose one specific target but one average representative of each group, considering the average orbital elements in semimajor axis, eccentricity, inclination and mean anomaly. On those baseline representatives, simplified permutations of the full complexity cases were done, to assess whether there were limits on the methods, in the assumptions or in the procedures. With these results, a "database" of outer problem targets was generated, upon which the transfer trajectories were designed. All the targets have been evaluated and the pipeline was robust enough to find solutions for every case reported.

To ease the explanation and the description of the method, one relevant case study is extracted, selecting one NEA case among the possibilities to continue the analysis: the planar and circular case of the "Amors" group, here in table 5 its initial orbital elements are reported, assuming the reference Epoch ET_0 as 2024-01-01 00:00:00.

Table 5: NEA Target Parameters

a [AU]	e [-]	i [deg]	Ω [deg]	ω [deg]	M [deg]
1.3645	0	0	0	0	196.2

The set of transfers is simply generated assuming Two-Body motion of the Earth and the target body around the Sun and exploiting Lambert problem method. In particular, having assigned a departure window of interest and a Time of Flight (TOF) span, a Porkchop Plot for the transfer can be easily built, as shown in fig. 9 for the case study reported. The Porkchop Plot from Earth to Target in 2BP direct Lambert transfer represent the ΔV cost of that manoeuvre departing at that date and taking that amount of time. The cost reported here is for a rendezvous mission. The cost associated to the ΔV of rendezvous is considered in full, while the ΔV associated to the departure from Earth is weighted by 0.5, meaning that the relative importance given to the departure is lower. This is because at this stage of the transfer, the algorithm knows little about how the spacecraft is meant to leave the Earth's space, and it's considering a direct injection into transfer orbit. But from the basis of this work, the departure will be associated to a WSB generated trajectory, with the purpose of being more efficient than a direct injection, and the same for the propellant cost associated to the departure.

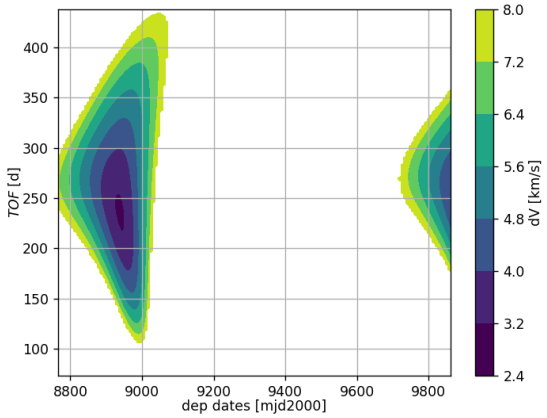

Fig. 9: Porkchop Plot of a Earth-NEA *Amor* Transfer, V_∞ Weighted

A reduced set of solutions is extracted from this, generating a small database of proper and valid solutions in 2BP, visualised as the red stars in fig. 10, that can be evaluated independently.

Thus far the problem is still under the 2BP framework, but all the analyses are provided in BCR4BP. For this reason, the transfer trajectories identified in the previous step need to be back-propagate in BCR4BP framework, starting from the arrival position to the target, that will not change, back in time to the Earth departure, using the same Time Of Flight. At this point, it's possible to see in fig. 11 that there will be some inconsistencies with the perfect match given by the 2BP analysis, bringing the departure point not anymore where the Earth is. For this reason, a small step of Differential Correction (DC) single shooting was used, to bring back the starting point at the Control Sphere around the Earth-Moon system, in the *xy* plane figure shown as the dotted red circle, reaching the condition at 2 million km.

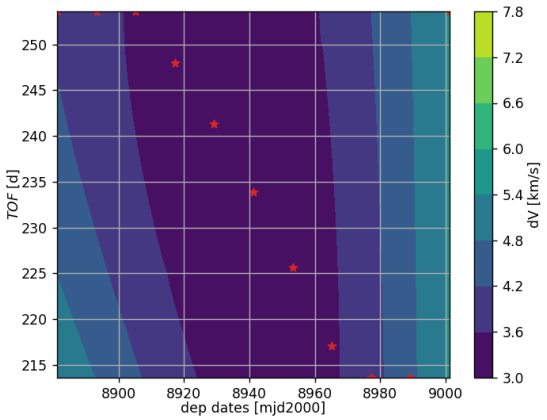

Fig. 10: Reduced Window Optimised Porkchop Plot of the Earth-NEA *Amor* Transfer, V_∞ Weighted

From this results, the newly corrected Outer Problem trajectories form the proper small database related to the Outer conditions to be matched by the Inner Problem WSB families trajectories, because now everything is reported in the same dynamical framework.

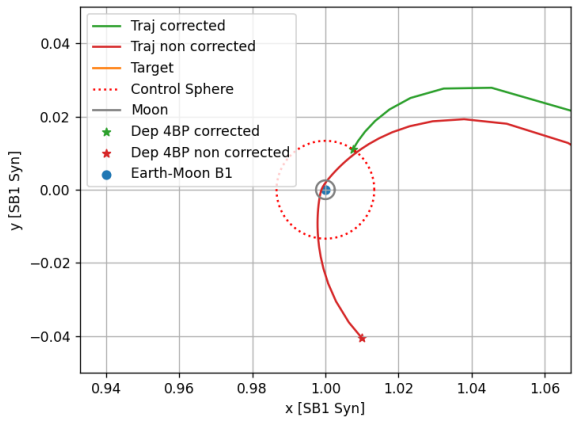

Fig. 11: Earth-NEA *Amor* Transfer 2BP, Back-Propagated in BCR4BP and Corrected to R_c

5.2 *Patching Procedure*

Among the multiple possible and feasible solutions is then selected the one that minimise the sum of the Lambert 2BP and the BCR4BP trajectory differential correction, in order to get the true minimum among these. The Inner Problem is used as a base to search for proper Outer Problem trajectory matching. For each family, an algorithm has been developed in order to find the best trajectory and the best one-impulse control to give at a specified point to reach the wanted parameters, and it will be described as follows.

1. One trajectory representative of the family is selected, privileging the ones with a pericentre where to apply a manoeuvre in the following steps. If this is not possible the manoeuvre will be applied to the apocenter.

2. A spectrum of manoeuvres is applied to that trajectory at its B_1 pericentre, in a variety of impulse magnitudes up to the maximum budget delegated to the on-board control, considered for now 0.5 km/s and 2 km/s; and in a variety of directions, considered now as radial, tangential and anti-radial (90°, 0°, -90°). All these options are propagated up to the control sphere, saving the most relevant matching parameters for later use as done in steps before. The procedure is depicted in fig. 12, showing the directions and the magnitudes of the impulses applied to a representative case taken as example, but the same is done on the other families and their trajectories.

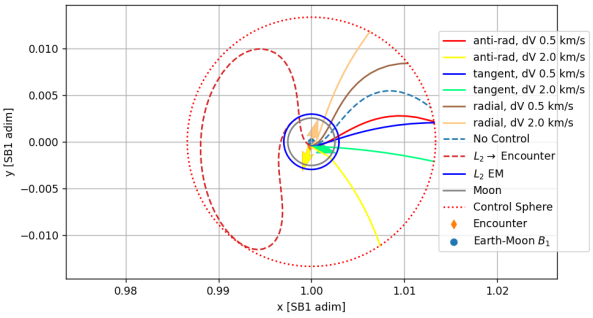

Fig. 12: Control Spectrum Example

3. A matrix of possible controlled trajectory is constructed and the one closest to the possible match is chosen. Having as objective the Outer Problem R_c condition to be patched, a multiple objective minimisation selection is applied, considering the difference in V_∞ in magnitude ($\Delta|V_\infty|$), the angular distance between them ($\Delta\theta_{R_c}$) and the different direction of their velocities ($\underline{V}_{inner} \sphericalangle \underline{V}_{outer}$), always at the control sphere. For each case, these quantities are then normalised between 0 and 1 and the minimum is selected as best first guess case.

4. If the family has a geometrical behaviour that brings all its trajectories toward a region of space not suited for that particular matching (angular difference at R_c between inner and outer trajectory $> \pi/4$), the family is discarded a priori from the analysis, because most probably will lead anyway to an expansive manoeuvre.

5. This spectrum control solution selected is then fed to another differential correction step, to actually meet the condition of the Outer Problem requested at the control sphere and produce a valid continuous path. The procedure is visually represented in fig. 13, where the main elements acting in the environment and the parameters used in the algorithm are shown. This optimisation proceeds minimising the residue related to the distance between the end point of the trajectory and the control sphere (in green in the legend), the difference in magnitude (yellow colour) and direction (in magenta) of the V_∞ at control sphere between the controlled trajectory and the outer problem request and the angular distance between the two always at R_c (in purple). These final solutions are saved in a database in order to be then post-processed during the final selection.

6. Among all the families solution, the one that has less overall sum residue of the differential correction step left at the end of the process, meaning the one that is the closest to the actual target request, is selected as best of all to patch the Outer Problem.

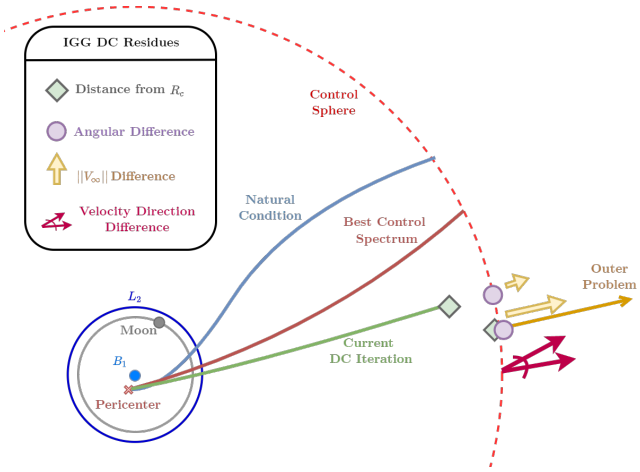

Fig. 13: Graphical Depiction of the IGG Differential Correction Procedure

The parameters are then extracted from this optimised solution and the results are presented in section 5.3 here following. For each case there are lots of solutions, but only few reference example are reported now.

5.3 *Patching Results*

Here the results proposed are the one related to the *Amor* NEA selected as case study at the beginning, showing how the algorithm works and what solution it proposed, selecting few different families as comparison.

The conditions deriving from the Outer Problem request at R_c are reported here in table 6. Those were found during the previous steps of Lambert Problem and Back Propagation in BCR4BP framework described before.

Table 6: Outer Problem Conditions to Match

$\mathbf{V_\infty}$ **[km/s]**	θ **[deg]**	$\hat{\mathbf{v}}_\mathbf{x}$ **[-]**	$\hat{\mathbf{v}}_\mathbf{y}$ **[-]**
2.479	39.71	0.7337	0.6794

The selected transfer trajectory was the one that cost $\Delta V_{2BP} = 3.107$ km/s from the Lambert 2BP and $\Delta V_{4BP} = 0.069$ km/s from the BCR4BP Back Propagation, for a total of $\Delta V_{TOT} = 3.176$ km/s. Keep in mind that this is not the actual cost because the injection associated ΔV was weighted by 0.5, but for the purpose of the selection now it has to be interpreted as an objective function and not as the real physical cost of the transfer, that will be delegated to a full optimisation in future steps.

Per each family, from the control spectrum propagation, the algorithm evaluates the selection metrics to be minimised, namely the difference in V_∞ in magnitude ($\Delta|V_\infty|$), the angular distance between them ($\Delta\theta_{R_c}$) and the different direction of their velocities ($\underline{V}_{inner} \sphericalangle \underline{V}_{outer}$), always at the Control Sphere. Not all the families made it through this filtering, because even with the best solution possible for that family, their $\Delta\theta$ was greater than 45° between the conditions, and for this reason discarded. After this passage, only 9 out of the total 14 families survived and have to be evaluated and corrected in order to yield a truly comparable result.

Following this initial filtering, the optimisation step can take place, trying to bring the difference between the request and the Inner Trajectory to zero. Sometimes the control overcome the 2 km/s limit or the radial/anti-radial limits that were imposed in the control spectrum step, but it's ok because nevertheless they will be initial guesses, just most expansive, less applicable and efficient. The optimised parameters are reported in table 7, for the α, ΔV and TOF parameters, along with the sum of residuals of the optimisation, parameter upon which the final selection will be made.

The cartesian plot 2D is hereby shown, demonstrating the outcome of the process in an efficient visual way. In the first picture fig. 14 the best condition of patching is shown, using the Family **F1** as selected one, where it's possible to notice all the comments done before and evaluate the actual matching: the difference in direction of the velocity is only 10.65°; the control applied is 1.221 km/s, well below the limit set and the lowest among the solutions; the V_∞ is com-

Table 7: Optimised Parameters and Final Residuals

Family	**Optimal** α [deg]	**Optimal** Δ **V** [km/s]	**Optimal TOF** [d]	**Sum Residuals [-]**
0	-35.64	2.649	11.04	0.011667
1	65.21	1.221	8.50	0.001698
3	84.09	2.190	8.68	0.001859
6	72.62	2.336	16.28	0.002294
7	-91.02	2.637	16.66	0.090657
9	79.83	2.053	8.43	0.002660
11	-234.57	1.627	6.18	0.034515
12	92.68	2.969	8.41	0.002013
14	-51.23	1.557	8.90	0.003068

pletely matched and also the position on the Control Sphere; the TOF has been reduced from the entry guess of the spectrum to 8.50 days because, being the control applied higher than the guessed one, the dynamic is faster.

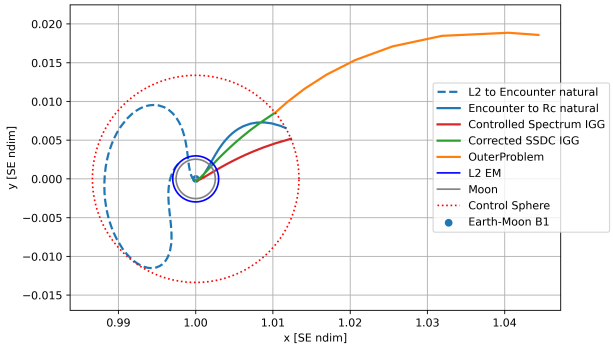

Fig. 14: Best Solution Patching NEA *Amor* Selected - Family **F1**

In the second picture fig. 15 is shown another good result coming out from the optimisation, relative to the Family **F3**. It's even better for what concern the velocity direction at 9.72°, but quite expensive compared to the first one at 2.19 km/s, over the initial guesses limit imposed from the control spectrum step. Also in this case the V_∞ and the position at the Control Sphere are completely matched, with a TOF reduced to 8.68 days.

In the last picture in fig. 16, one of the converged results that would perform badly. In the case of the Family **F11**, the patching gives as results a trajectory that continue to orbit around the Earth at a very close distance, making completely useless the process. From the algorithm point of view, the end point of this trajectory is still aligned with the Outer Problem, this is the reason why it was not discarded in the first pruning step. But there are also other reasons why this solution should not be considered: the totally out-

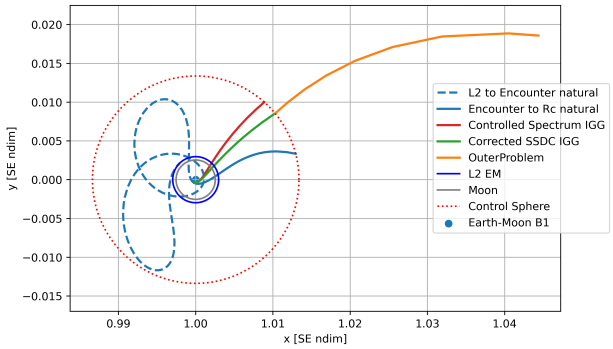

Fig. 15: Good Solution Patching NEA *Amor* Selected - Family **F3**

lier Optimal α obtained, very far from the control spectrum limits and guess, meaning that the obtained trajectory will be different from the proposed one; and the relatively high overall residue, one order of magnitude more than the best patching solution. At this point the other patching metrics shouldn't even be considered, but it's possible to see that the V_∞ has one of the worst match and the TOF is the lowest among the results.

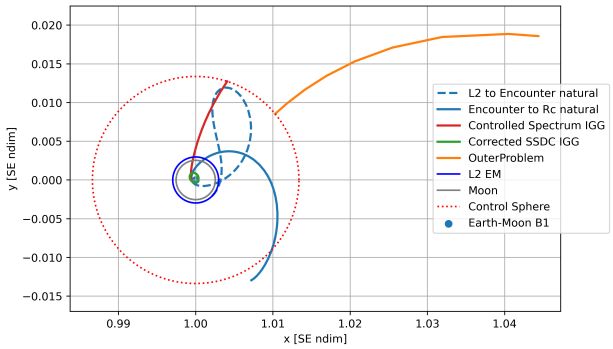

Fig. 16: Bad Solution Patching NEA *Amor* Selected - Family **F11**

6. CONCLUSIONS

In this paper, a new methodology for the generation and classification of weak-stability boundaries escape trajectories have been presented, along with the application for a relevant NEA case.

The problem has been splitted into Inner and Outer Problem and the initial conditions databases have been generated independently: for the WSB escape family trajectories, through machine learning clustering and for the targets scenarios, through 2BP Lambert's solution, Porkchop Plots and

BCR4BP differential correction.

Then the actual patching procedure was presented and discussed, matching the geometrical and dynamical characteristics at the Control Surface. The mechanisms of initial guess generation was finally applied to a NEA rendezvous mission example, reporting the results.

The method appears to be flexible and efficient, since the escape conditions can be built once and then used for different mission scenarios. Moreover, the clustering into families gives the possibility to filter the database upon certain characteristics a priori of the optimisation, ultimately leading to a smaller subset of valid and cost-effective initial guesses to be processed. The application of the patching conditions, passed through the control spectrum step, guarantees a fast convergence of the differential correction procedure, allowing for a fast identification of suitable escape trajectories from the cislunar space.

REFERENCES

[1] E. Belbruno and J. Miller. A ballistic lunar capture trajectory for the japanese spacecraft hiten. *Jet Propulsion Laboratory*, 1990.

[2] Edward Belbruno, Marian Gidea, and Francesco Topputo. Weak stability boundary and invariant manifolds. *SIAM J. Applied Dynamical Systems*, 9:1061–1089, 01 2010.

[3] Stephen Broschart, Min Kun, J Chung, Sara Hatch, Jin Ma, Theodore Sweetser, Stacy Weinstein-Weiss, Vassilis, and Angelopoulos. Preliminary trajectory design for the artemis lunar mission. volume 135, 08 2009.

[4] Christian Circi and Paolo Teofilatto. Weak stability boundary trajectories for the deployment of lunar spacecraft constellations. *Celestial Mechanics and Dynamical Astronomy*, 95:371–390, 2006.

[5] J. R. Doll and F. W. Gobetz. A survey of impulsive trajectories. *AIAA Journal*, 7(5):801–834, May 1969.

[6] ESA. How smart-1 has made european space exploration smarter, 25 August 2022.

[7] Fabio Ferrari, Michèle Lavagna, and Kathleen C. Howell. Dynamical model of binary asteroid systems through patched three-body problems. *Celestial Mechanics and Dynamical Astronomy*, 125(4):413–433, August 2016.

[8] Márton Geda, Ron Noomen, and Florian Renk. Massive parallelization of trajectory propagations using gpus. *TU Delft Aerospace Engineering*, 2019-01-13.

[9] Cristian Greco, Marilena Di Carlo, Lewis Walker, and Massimiliano Vasile. Analysis of neos reachability with nano-satellites and low-thrust propulsion. 06 2018.

[10] Michihiro Matsumoto and Jun'ichiro Kawaguchi. Escape Trajectory and Connection to Interplanetary Voyage from the Sun-Earth L2 Point. *Space Technology*, 4:43–52, January 2006.

[11] Masaki Nakamiya and Hiroshi Yamakawa. *Earth Escape Trajectories Starting from L2 Point*.

[12] NASA Jet Propulsion Laboratory. Solar system dynamics - small-body database query. California and Institute of Technology.

[13] Andrea Pasquale, Michèle Lavagna, and Florian Renk. Cislunar escape trajectories through patched sun-earth/earth-moon three-body problem. 10 2021.

[14] F. Pedregosa, G. Varoquaux, A. Gramfort, V. Michel, B. Thirion, O. Grisel, M. Blondel, P. Prettenhofer, R. Weiss, V. Dubourg, J. Vanderplas, A. Passos, D. Cournapeau, M. Brucher, M. Perrot, and E. Duchesnay. Scikit-learn: Machine learning in Python. *Journal of Machine Learning Research*, 12:2825–2830, 2011.

[15] Marco B. Quadrelli, Lincoln J. Wood, Joseph E. Riedel, Michael C. McHenry, MiMi Aung, Laureano A. Cangahuala, Richard A. Volpe, Patricia M. Beauchamp, and James A. Cutts. Guidance, navigation, and control technology assessment for future planetary science missions. *Journal of Guidance, Control and Dynamics*, May 9, 2015.

[16] Daniele Romagnoli and Christian Circi. Earth–moon weak stability boundaries in the restricted three and four body problem. *Scuola di Ingegneria Aerospaziale, Università di Roma La Sapienza*, October 2008.

[17] Ralph Roncoli and Kenneth Fujii. Mission design overview for the gravity recovery and interior laboratory (grail) mission. 08 2010.

[18] Stephen T. Scheuerle. Construction of ballistic lunar transfer in the earth-moon-sun system. Master's thesis, Purdue University School of Aeronautics and Astronautics, West Lafayette, Indiana, USA, May 2021.

[19] Thomas Smith and Natasha Bosanac. Constructing motion primitive sets to summarize periodic orbit families and hyperbolic invariant manifolds in a multibody system. *Celestial Mechanics and Dynamical Astronomy*, 134, 02 2022.

[20] Keita Tanaka and Jun'ichiro Kawaguchi. Escape trajectories from the l2 point of the earth-moon system. *TRANSACTIONS OF THE JAPAN SOCIETY FOR AERONAUTICAL AND SPACE SCIENCES*, 57:238–244, 07 2014.

[21] Michael Thompson, Ethan Kayser, Jeffrey Parker, Connor Ott, Matthew Bolliger, Thomas Gardner, and Bradley Cheetham. Navigation design of the capstone mission near nrho insertion. 08 2021.

[22] Kuninori Uesugi, Jun'ichiro Kawaguchi, Nobuaki Ishii, Miwako Shuto, Hiroshi Yamakawa, and Kimie Tanaka. Follow-on mission description of hiten. -1:1723–1728, 01 1992.

[23] Lucas Vendramin, Ricardo J. G. B. Campello, and Eduardo R. Hruschka. Relative clustering validity criteria: A comparative overview. *Statistical Analysis and Data Mining: The ASA Data Science Journal*, 3(4):209–235, 2010.